Available online at www.sciencedirect.com

ScienceDirect

Energy Procedia 126 (201709) 778–785

Energy Procedia

www.elsevier.com/locate/procedia

72nd Conference of the Italian Thermal Machines Engineering Association, ATI2017, 6-8 September 2017, Lecce, Italy

Efficient CFD evaluation of the NPSH for centrifugal pumps

M. Lorusso[a,*], T. Capurso[a], M. Torresi[a], B. Fortunato[a], F. Fornarelli[a], S.M. Camporeale[a], R. Monteriso[b]

[a] *Department of Mechanics, Mathematics and Management (DMMM), Politecnico di Bari University, Viale Japigia 182, 70126, Bari, Italy*
[b] *GE Oil and Gas - Nuovo Pignone, Via II Tratto e Inizio Statale 98 Modugno 10, 70132, Industrial area of Bari, Italy*

Abstract

This paper provides the reader with guidelines for the definition of coarse but effective meshes on reduced computational domains in order to accurately evaluate the drop curves and the $NPSH_{3\%}$ of centrifugal pumps by means of CFD. The procedure has been validated against experimental data, carried out on single stages of multi-stage centrifugal pumps, and numerical data obtained by a monodimensional model. Thanks to the proposed procedure, without any detriment to the accuracy, a significant computational cost reduction has been experienced with respect to simulations performed on complete stages.

Peer-review under responsibility of the scientific committee of the 72nd Conference of the Italian Thermal Machines Engineering Association

Keywords: Centrifugal pump; NPSH; Drop curve; CFD; RANS.

1. Introduction

The functionality and performance of a pump strongly depends on its hydrodynamics. Cavitation is a critical aspect to be taken into account in the design of hydraulic pumps. Cavitation can significantly reduce the efficiency, generate vibration and noise, and damage the pump.

In recent years, an increasing amount of information has been available in the literature about cavitation [1-4]. Researchers are particularly interested in the mechanisms, which induce cavitation, and in the main characteristics of

* Corresponding author.
E-mail address: michele.lorusso@hotmail.com

1876-6102
Peer-review under responsibility of the scientific committee of the 72nd Conference of the Italian Thermal Machines Engineering Association
10.1016/j.egypro.2017.08.262

a cavitating flows; for instance, several experimental tests have been carried out on Venturi ducts [5-6] and hydrofoils [7-8]. The main purpose of all these works has been the development of theoretical models helping in the prediction of the basic cavitation mechanisms. In addition, a number of other investigations on two-phase cavitating flows in pumps is available [9-16]. Moreover, experimental investigations can be found, showing the use of particle image velocimetry (PIV) and high speed digital camera for visual cavitation [17-24]. The experimental data are essential for validating the numerical models.

Currently, Computational Fluid Dynamics (CFD) represents a common practice to design and optimize hydraulic pumps, since it can improve pump design, whilst reducing development cost, and accelerating the time to the market.

The pump industry supports research, in order to progress in understanding and predicting the cavitation phenomenon. In industrial practice, the cavitation process is quantified by means of the Net Positive Suction Head (NPSH). Actually, there are several criteria to evaluate the NPSH, but the most frequently used is the $NPSH_{3\%}$ because it is the easiest to be measured [3].

Several numerical models for calculating the $NPSH_{3\%}$ and evaluating the drop curves of pumps can be found. Generally, these models consider the entire runner as the computational domain showing a great predictability of the $NPSH_{3\%}$. However, these model require a high computational cost, therefore it has been sought an alternative and less expensive approach.

For the initial design of a pump, researchers and technical engineers of Industrial Companies have developed their own monodimensional tools. Thanks to their very low computational cost, the monodimensional model allows one to roughly evaluate the pumps performance in a very short period of time.

In this paper the main purpose consists in developing and validating an efficient procedure in order to evaluate both the drop curve and the $NPSH_{3\%}$ via numerical investigations.

First of all, under the assumption of rotational periodicity, the simulation domain has been limited to a single blade vane. Moreover, portions of both suction and discharge annuli have been considered (see Fig. 1a) in order to simplify the boundary condition assignment. By means of the ICEM CFD software, four mesh configurations, which differ in terms of cell numbers across the boundary layer and local mesh densities, have been defined in order to carry out a mesh sensitivity analysis.

The CFX software has been used for solving the 3D steady state Reynolds-Averaged Navier–Stokes equations (RANS). The k-ω SST model has been chosen for turbulence closure. In order to take into account cavitation, the Rayleigh-Plesset equation is solved according to the Zwart-Gerber-Belamri [25] model. The following paragraphs will describe the mesh preparation procedure, the model setting by means of the Ansys CFX-Pre, the post-processing and result validation.

Nomenclature

NPSH	Net Positive Suction Head (m)
p_{in}^0	Total pressure at inlet (Pa)
p_{out}^0	Total pressure at outlet (Pa)
p_{sat}	Saturation pressure (Pa)
ρ	Water density (kg/m^3)
g	Gravity acceleration (m/s^2)
H	Head (m)

2. Mesh

A single stage (in particular, the first stage) of a multi-stage pump with both suction and discharge annuli has been considered. Actually, the computational domain has been limited to a single blade vane (see Fig. 1a). The computational domain has been first reproduced by CAD and then exported into the ICEM CFD grid generator for mesh discretization. The computational domain has been confined by two periodic surfaces in the middle of two

consecutive vanes. 4 meshes, with different criteria, have been created. The same procedure has been applied for other 16 pumps.

In order to create a mesh, ANSYS ICEM CFD requires that the model contains a closed volume. To verify this, it is necessary to confirm that the geometry is free of any flaws that would otherwise inhibit an optimal mesh creation.

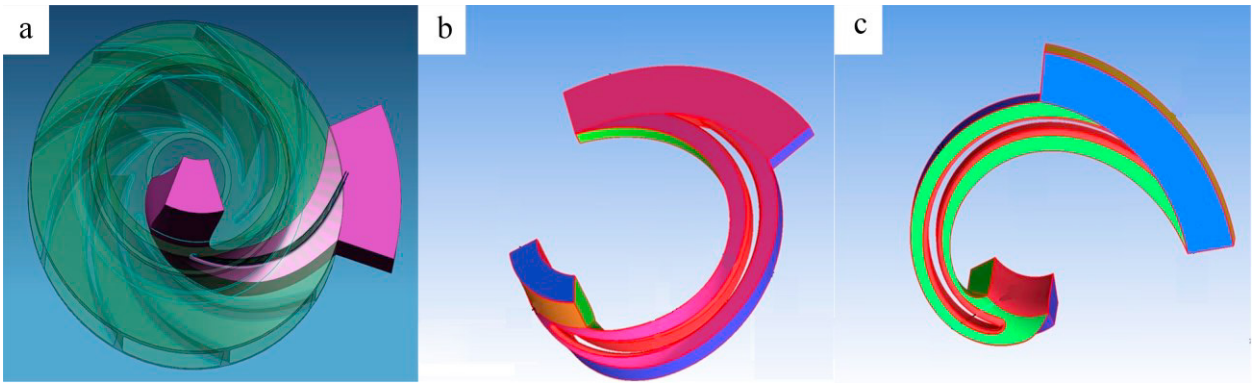

Fig. 1 Visualization of the computational domain

The mesh generation takes into account four criteria (see Table 1). 1) The "Global scale factor", which has been set equal to 1 for all the meshes; 2) the "Maximum element seed size", which controls the global size of the largest element; 3) the "Refinement", which defines the number of edges that would fit along a curvature radius if that radius is extended out to 360 degrees. Actually, this last control is generally used to avoid having too many elements along a given curve or surface.

The Body-Fitted Cartesian mesh generator can create a layer of hexa-elements parallel to the wall. These are necessary for properly capturing the flow inside the boundary layers. In the Part Mesh Setup dialog box, it is possible to enable the prism meshing for the appropriate parts and the number of offset layers. The structured mesh is determined on a part by part basis, so parts must be created and surfaces appropriately assigned. The surfaces/parts selected to create prism layers are all wet surface. In the Part Mesh Setup dialog it's possible to specify the "Local maximum element" sizes. In both mesh 1 and mesh 2, a "local maximum element size" around the blade equal to 2 has been defined.

Tetra/Mixed mesh type has been used to complete the domain meshing. In CFX there are three different mesh methods available for Tetra/Mixed meshing: Robust (Octree), Quick (Delaunay), and Smooth (Advancing Front). During the computational domain discretization, first the Robust and then the Smooth Tetra/Mixed meshing algorithm has been used. The former ensures refinement of the mesh where necessary (based on the entity size, the curvature and the proximity based refinement settings), but maintains larger elements where possible. The second one generates a Tetra mesh using a bottom-up meshing approach. The surface mesh is created as defined by the Global Mesh Setup settings. The volume mesh is generated from the surface mesh. This meshing method results in a more gradual change in the element size. However, the initial surface mesh should be of fairly high quality.

Table 1 Main parameters for the mesh setup

Mesh	Global max element size	Refinement	Prism total height [mm]	Local max size [mm]	Prism layers	Prism ratio	Size density	Ratio density	Width density	(N° elements) / (N° elements mesh 4)
1	4	20	1	BLADE=2	6	1.2	1	1.2	15	5
2	4	20	1	BLADE=2	6	1.2	-	-	-	4
3	5	16	0.5	-	3	1.6	-	-	-	2.5
4	7	10	-	-	-	-	-	-	-	1

Mesh 1 represents the mesh setup with the highest number of cells. A local mesh refinement at the blade leading edge has been implemented. The “size density” in Table 1 specifies the local maximum mesh size that has been employed within the refined region. Other two parameters are worth to be evidenced: the “Ratio density” and the “Width density”, which influence the tetrahedral cell growth ratio away from the density region and the radius of the region, respectively. As it will be shown in the following sections, the density function allows one to calculate more accurately the cavity bubble on the leading edge than meshes without the local refinement.

Views of both Mesh 1 and 4 are illustrated in Fig. 2. It is worth to notice that Mesh 4 does not have prism layers and that the grid element size is generally bigger in Mesh 1 than in Mesh 4. In Fig. 2c, the local mesh refinement used in Mesh 1 is clearly visible.

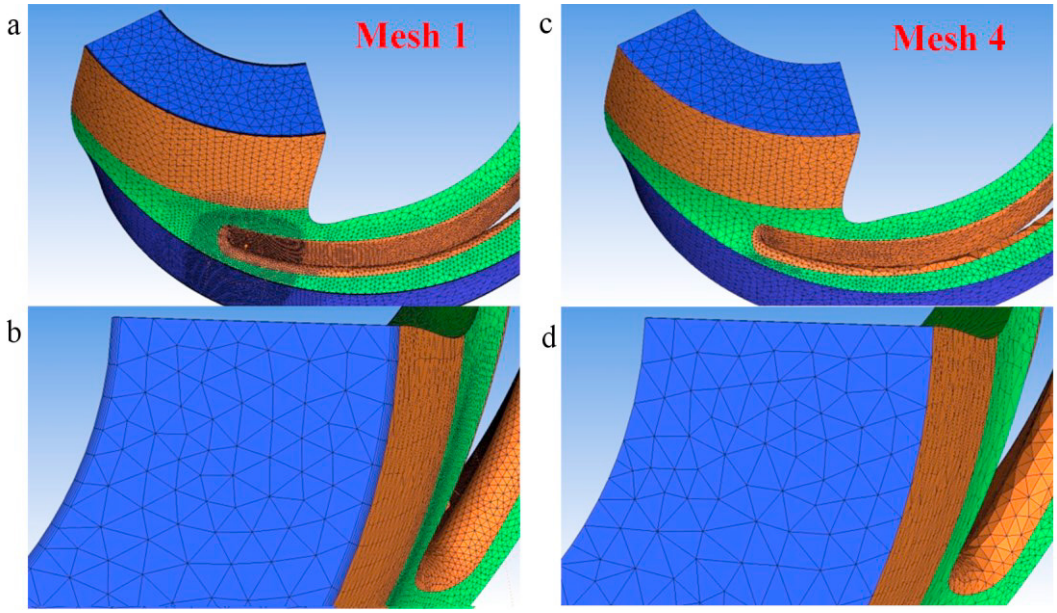

Fig. 2 Visualization of Mesh 1 (a and b) and Mesh 4 (c and d).

3. Numerical approach

All the numerical simulations are steady state with the application of a *High resolution* advection scheme for all the variables. A convergence criterion with RMS residual type has been used, moreover the minimum value for the residues have been set equal to 10^{-6}. The implemented turbulence model is the k-ω Shear Stress Transport (SST). This model accounts for the transport of the turbulent shear stress and gives highly accurate predictions of the onset and the amount of flow separation under adverse pressure gradients.

In CFX, the Rayleigh-Plesset model is implemented in the multi-phase framework as an interphase mass transfer model. For cavitating flows, the homogeneous multi-phase model is used. The two phases consist in water and water vapour at 25°C, hence the saturation pressure has been set equal to 3575 Pa. The Rayleigh-Plesset equation is solved according to the Zwart-Gerber-Belamri [25] model imposing the default parameters.

3.1. Boundary conditions

The boundary conditions are the following: total pressure at the inlet, mass flow rate at the outlet, no-slip and adiabatic conditions enforced on all the wet walls and scalable wall functions for the near-wall regions. All solid surfaces of the impeller are named *rotating walls* to simulate the rotation. The surfaces near the outlet are defined free-slip. Doing so, a null stress wall tensor on these surfaces is imposed, avoiding erroneous results on the assessment of the impeller head. Finally, the two periodic surfaces were set as rotational periodic surfaces.

The total inlet pressure and inlet velocity versor (with respect to the cylindrical reference frame) with an average turbulence intensity of 5% have been set at the inlet section. The swirl component of the velocity versor has been defined according to the pre-swirl outlet velocity angle; no radial velocity component have been considered.

The numerical analyses have been set as follow: firstly, a single-phase calculation has been run with a value of the total pressure, imposed at inlet, 6-8 times greater than the pressure corresponding to the $NPSH_{3\%}$ evaluated by means of a monodimensional model. Subsequently, multi-phase calculations have been run. In the first of these the boundary conditions are exactly the same of the single-phase simulation, then, in the following simulations, the total pressure imposed at the inlet is continuously reduced, at first with larger steps. Basically, the assigned total pressure values are distributed according to a hyperbolic function, as shown in Fig. 3. In this way, the knee of the drop curve can be more accurately estimated and hence the value of $NPSH_{3\%}$.

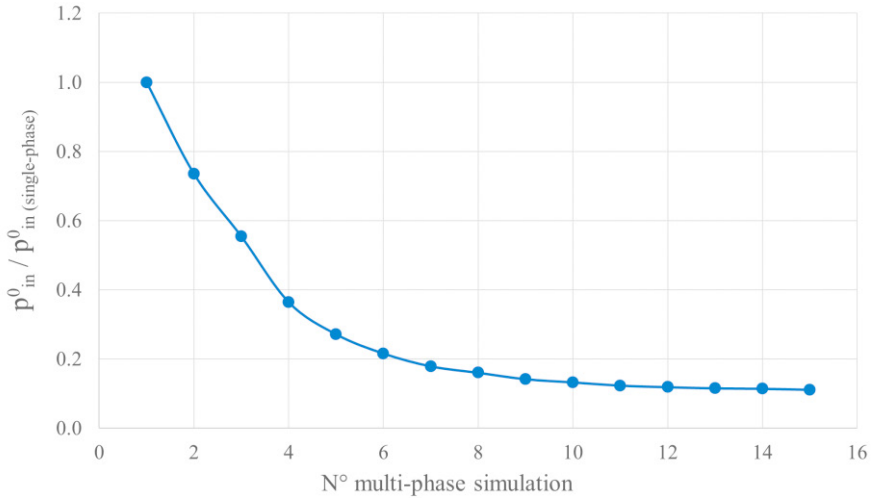

Fig. 3 Values of the total pressure imposed at the inlet boundary during the construction of the pressure drop curve

4. Numerical results

For each simulation, the head value, *H*, is calculated as follows:

$$H = \frac{(p^0_{out} - p^0_{in})}{\rho g} \tag{1}$$

Decreasing the inlet total pressure, p^0_{in}, the cavitation bubble volume increases at the leading edge and the head, *H*, provided by the impeller, which initially is not significantly affected by the presence of cavitation, decreases.

When the head, *H*, decreases by the 3% with respect to the value computed in absence of cavitation (single-phase), the value of $NPSH_{3\%}$ can be defined. The NPSH is defined in Eq.2:

$$NPSH = \frac{(p^0_{in} - p_{sat})}{\rho g} \tag{2}$$

In Fig. 4 the drop curves corresponding to the four meshes are reported. For the four meshes, the value of the head is different. Actually, it increases with the number of cells, coherently to the findings of Q. Fu *et al.* [10]. In fact, by increasing the number of cells, the solver calculates more accurately the flow. Moreover, the percentage difference of head is evaluated and compared to the single-phase value (Fig.5). The drop curves computed by means of the four meshes, are very close as well as the value of the $NPSH_{3\%}$. This means that even using Mesh 4 (the coarser one), the $NPSH_{3\%}$ can be correctly estimated.

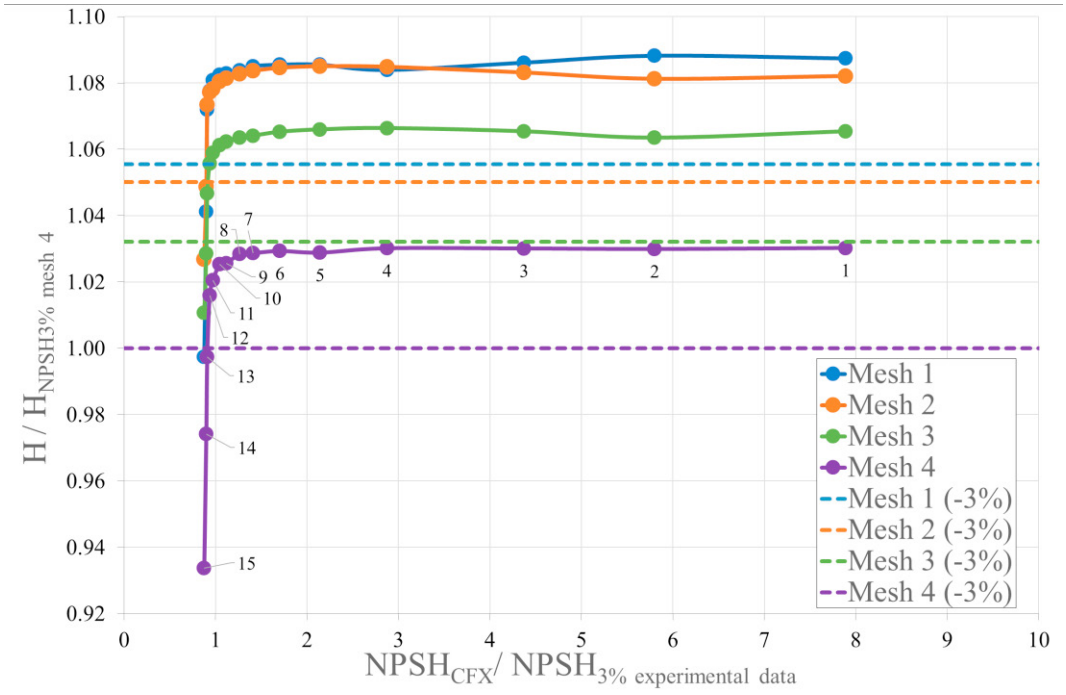

Fig. 4 Computed heads during a pressure drop test and 3% head drop lines (with respect to single-phase) for the 4 meshes

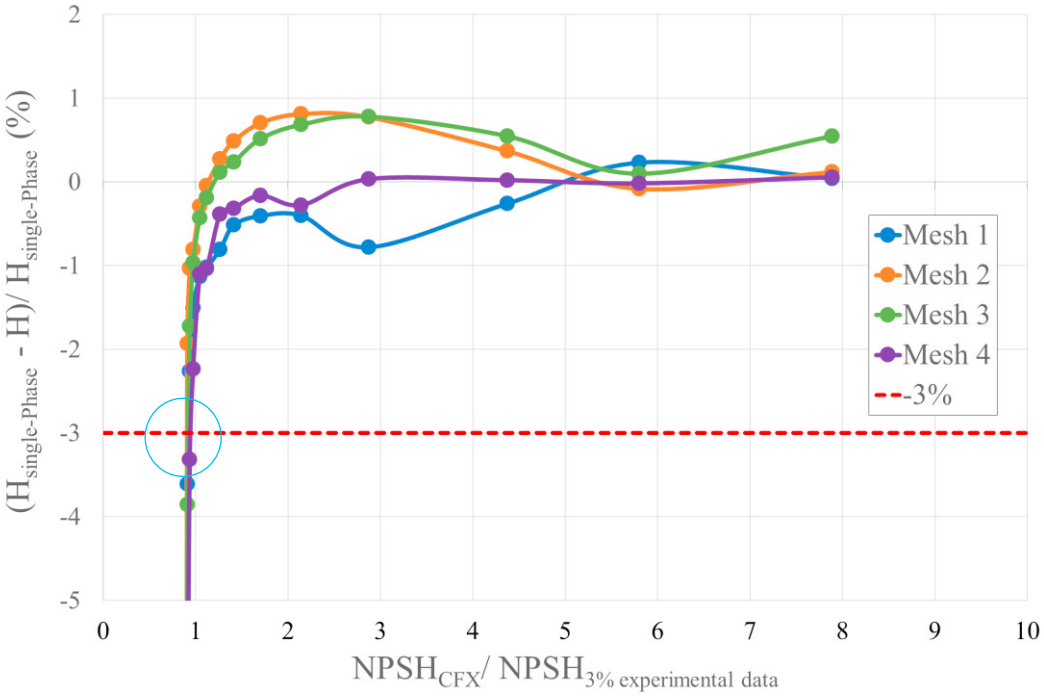

Fig. 5 Pressure drops and 3% head drop lines (with respect to single-phase) for the 4 meshes

The values of the $NPSH_{3\%}$ for other 16 impeller geometries have been calculated following the same rules of Mesh 4 and compared with the corresponding values estimated by means of a monodimensional model. Fig. 6a

represents in abscissa the value of the $NPSH_{3\%}$ calculated by means of CFX, whereas in ordinate the value calculated by means of the one-dimensional model. In the graph, the 45° black dashed line represents the line where the results would lie if both CFX and the monodimensional model would have given the same values. In Fig. 6a, it is worth to notice that the monodimensional model overestimates the $NPSH_{3\%}$, which means that the monodimensional model results can be used only in the initial design phase.

The Fig. 6b compares the values obtained with CFX with the experimental data of 7 impeller geometries.

Instead, when comparing the CFX results with respect to the experimental data (see Fig. 6b), it is possible to verify the high accuracy in evaluating the $NPSH_{3\%}$ with a very limited computational effort.

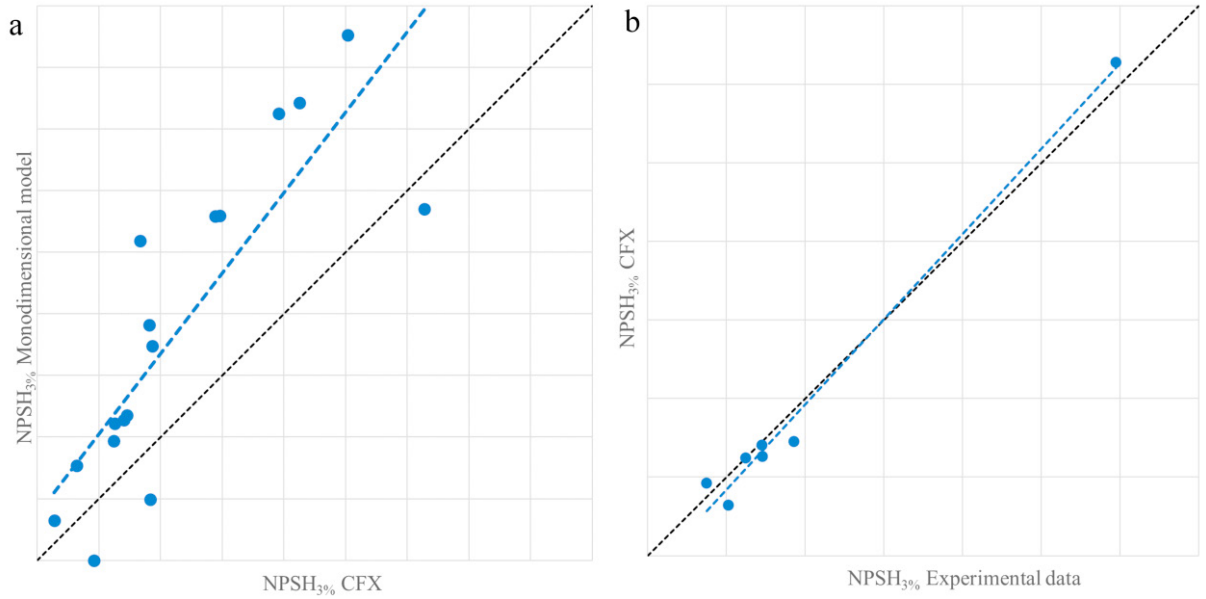

Fig. 6 Comparison of CFX results against the monodimensional model results (a) and the experimental data (b).

5. Conclusion

In this work an efficient procedure to evaluate the $NPSH_{3\%}$ for centrifugal pumps by means numerical simulations has been developed. The numerical results were compared with both a monodimensional model and experimental data. The first comparison (Fig. 6a) has highlighted that the monodimensional model tends to overestimate the $NPSH_{3\%}$ value compared to CFX results. From the second comparison (Fig. 6b) it is significant to see how the CFX results are very accurate with respect to experimental data.

It has been shown how the number of cells has a small influence on the $NPSH_{3\%}$ evaluation. On the contrary it affects the head estimation. The head increases asymptotically with the increase of the number of cells. This is due to the fact that, with a greater number of elements, the accuracy of the simulation improves.

In conclusion, it is possible to say that for an accurate evaluation of both head and $NPSH_{3\%}$ values a grid similar to Mesh 1 is needed, whereas if the main focus is to save computational time and to have a fairly accurate estimation of the $NPSH_{3\%}$, we can use a grid similar to Mesh 4.

Acknowledgement

The authors wish to thank GE Oil and Gas – Nuovo Pignone for the opportunity given to M. Lorusso to attend a six-month internship at their plant.

References

[1] CE Brennen, (1995) "Cavitation and bubble Dynamics." *Oxford engineering & sciences series 44. New York: Oxford University Press.*

[2] CE Brennen, (2005) "Fundamentals of multiphase flows." *Oxford University Press.*

[3] CE Brennen, (1994) "Hydrodynamics of pumps." *Concepts ETI, Inc. and Oxford University Press.*

[4] JF Gülich, (2010) "Centrifugal pumps." *Springer-Verlag Berlin Heidelberg. Second edition:* 259-335

[5] S Barre, J Rolland, G Boitel, E Goncalves and R Fortes Patella, (2008) "Experiments and modeling of cavitating flows in venturi: attached sheet cavitation." *European Journal of Mechanics B/Fluids*

[6] B Stutz and JL Reboud, (1997) "Experiments one unsteady cavitation. "*Springer-Verlag Berlin Heidelberg. Exp. Fluids 22:* 191–198.

[7] A Cervone, C Bramanti, E Rapposelli, L d'Agostino, (2006) "Thermal cavitation experiments on a NACA 0015 hydrofoil." *J. Fluids Eng. 128 (2)*: 326–331.

[8] M Dular, R Bachert, B Stoffel and B Širok, (2004) "Experimental evaluation of numerical simulation of cavitating flow around hydrofoil" *European Journal of Mechanics B/Fluids 24* (2005): 522–538.

[9] P Dupont and E Casartelli, (2002), "Numerical prediction of the cavitation in pumps." *ASME 2002 Fluids Engineering Division Summer Meeting.*

[10] Q Fu, F Zhang, R Zhu and B Heb (2016), "A systematic investigation on flow characteristics of impeller passage in a nuclear centrifugal pump under cavitation state" *Annals of Nuclear Energy.*

[11] H Ding, FC Visser, Y Jiang and M Furmanczyk (2009), "Demonstration and validation of a 3D CFD simulation tool predicting pump performance and cavitation for industrial applications" *Proceedings of the ASME 2009 Fluids Engineering Division Summer Meeting.*

[12] H Liu, J Wang, Y Wang, H Zhang and H Huang (2014), "Influence of the empirical coefficients of cavitation model on predicting cavitating flow in the centrifugal pump." *Int. J. Nav. Archit. Ocean Eng. (2014) 6*: 119-131.

[13] I Bilus and A Predin, (2009),"Numerical and experimental approach to cavitation surge obstruction in water pump." *International Journal of Numerical Methods for Heat & Fluid Flow, Vol. 19 Iss 7*: 818 – 834

[14] X Guo, Z Zhu, B Cui and Y Li, (2015), "Effects of the short blade locations on the anti-cavitation performance of the splitter-bladed inducer and the pump." *Chinese Journal of Chemical Engineering Volume 23, Issue 7. (2015)*: 1095–1101

[15] R Hirschi, P Dupont, F Avellan, JN Favre, JF Guelich and E Parkinson, (1998), "Centrifugal pump performance drop due to leading edge cavitation: numerical predictions compared with model tests." *J. Fluids Eng 120(4)*: 705-711

[16] B Schiavello and FC Visser (2009), "Pump cavitation - various NPSHR criteria, NPSHA margins, and impeller life expectancy." *Proceedings of the Twenty-Fifth International Pump Users Symposium, 23 – 26th Feb 2009, Houston, Texas, USA*: 113-144.

[17] Y Wang, H Liu, D Liu, S Yuan, JWang and L Jiang (2016), "Application of the two-phase three-component computational model to predict cavitating flow in a centrifugal pump and its validation." *Computers and Fluids 131 (2016):* 142–150.

[18] O Coutier-Delgosha, R Fortes-Patella, J L Reboud, M Hofmann and B Stoffel, (2004) "Experimental and Numerical Studies in a Centrifugal Pump With Two-Dimensional Curved Blades in Cavitating Condition." *J. Fluids Eng 125(6)*: 970-978.

[19] J Wang, Y Wang, H Liu, H Huang and L Jiang, (2015),"An improved turbulence model for predicting unsteady cavitating flows in centrifugal pump." *International Journal of Numerical Methods for Heat & Fluid Flow, Vol. 25 Iss 5*: 1198 – 1213

[20] R Balasubramanian, S Bradshaw and E Sabini, (2011), "Influence of impeller leading edge profiles on cavitation and suction performance." *Proceedings of the 27th International Pump Users Symposium (2011)*: 12-15.

[21] AAB Al-Arabi, SMA Selim, R Saidur, SN Kazi and GG Duffy, (2011), "Detection of Cavitation in Centrifugal Pumps." *Australian Journal of Basic and Applied Sciences, 5(10)*: 1260-1267

[22] Y Fu, J Yuan, S Yuan, G Pace, L d'Agostino, P Huang and X Li, (2014), "Numerical and Experimental Analysis of Flow Phenomena in a Centrifugal Pump Operating Under Low Flow Rates." *J. Fluids Eng 137(1), 011102*

[23] L Hou-lin, L Dong-xi, W Yong, W Xian-fang, WANG Jian and DU Hui, (2013), "Experimental investigation and numerical analysis of unsteady attached sheet cavitating flows in a centrifugal pump." *Journal of Hydrodynamics, Ser. B Volume 25, Issue 3*: 370-378

[24] B Antonio, M De Lucia and P Nesi, (1998), "Real-Time Detection of Cavitation for Hydraulic Turbomachines." *Real-Time Imaging Volume 4, Issue 6*: 403-416

[25] PJ Zwart, AG Gerber, and T Belamri, (2004) "A two-phase model for predicting cavitation dynamics." *ICMF 2004 International Conference on Multiphase Flow. Yokohama*: 152.